Research article

Cristian Ciracì*, Radoslaw Jurga, Muhammad Khalid and Fabio Della Sala

Plasmonic quantum effects on single-emitter strong coupling

https://doi.org/10.1515/nanoph-2019-0199
Received June 27, 2019; revised July 18, 2019; accepted July 21, 2019

Abstract: Coupling between electromagnetic cavity fields and fluorescent molecules or quantum emitters can be strongly enhanced by reducing the cavity mode volume. Plasmonic structures allow light confinement down to volumes that are only a few cubic nanometers. At such length scales, nonlocal and quantum tunneling effects are expected to influence the emitter interaction with the surface plasmon modes, which unavoidably requires going beyond classical models to accurately describe the electron response at the metal surface. In this context, the quantum hydrodynamic theory (QHT) has emerged as an efficient tool to probe nonlocal and quantum effects in metallic nanostructures. Here, we apply state-of-the-art QHT to investigate the quantum effects on strong coupling of a dipole emitter placed at nanometer distances from metallic particles. A comparison with conventional local response approximation (LRA) and Thomas-Fermi hydrodynamic theory results shows the importance of quantum effects on the plasmon-emitter coupling. The QHT predicts qualitative deviation from LRA in the weak coupling regime that leads to quantitative differences in the strong coupling regime. In nano-gap systems, the inclusion of quantum broadening leads to the existence of an optimal gap size for Rabi splitting that minimizes the requirements on the emitter oscillator strength.

Keywords: plasmonics; strong coupling; nonlocal response; hydrodynamic model; fluorescence.

1 Introduction

A quantum emitter placed nearby a plasmonic structure shows a drastic change [1–8] in its radiation dynamic properties compared to its interaction with the vacuum fields. Such light-atom interactions are of particular interest for applications in quantum computation [9, 10], biosensing [11, 12], nanolasing [13] and active plasmonic devices [14]. When the coupling of a photon emitter with the surrounding plasmonic cavity is large enough so that the energy exchange happens before it is lost (or decayed) in the system, it is possible to enter the strong coupling regime where the emitter can reversibly exchange photons with the close-by environment, leaving a signature in the optical emission spectra widely known as Rabi splitting [15–18].

Strong coupling in light-matter interactions requires highly enhanced optical fields and small cavity volumes [19]. The latest developments in the nanotechnology and nanofabrication techniques [20–23] allow the engineering of metallic structures supporting localized surface plasmons able to squeeze light in ever smaller nanovolumes, thus, offering an excellent platform to explore strong electromagnetic coupling in plasmonic cavities [19, 24].

The largest optical field confinement can be achieved in metallic structures with a few- nanometer or even subnanometer inter-particle distances [25–27]. Recent experiments on systems characterized by such small length scales have shown phenomena that go beyond classical electrodynamics [28–34]. These phenomena are caused by purely quantum mechanisms [35], such as electron spill-out, quantum tunneling and confinement, or by semi-classical effects [36], such as the nonlocal optical response of free-electrons.

Nonlocal effects can be formally described by the general relation between the displacement and electric fields, $\mathbf{D}(\mathbf{r}, \omega) = \int \varepsilon(\mathbf{r}, \mathbf{r}'; \omega)\mathbf{E}(\mathbf{r}', \omega)d\mathbf{r}'$. Typically, the optical response is characterized by short-range interactions, which in most cases can be approximated by a

***Corresponding author: Cristian Ciracì,** Center for Biomolecular Nanotechnologies, Istituto Italiano di Tecnologia, Via Barsanti, 73010 Arnesano, Italy, e-mail: cristian.ciraci@iit.it. https://orcid.org/0000-0003-3349-8389
Radoslaw Jurga: Center for Biomolecular Nanotechnologies, Istituto Italiano di Tecnologia, Via Barsanti, 73010 Arnesano, Italy; and Dipartimento di Matematica e Fisica "E. De Giorgi", Università del Salento, Via Arnesano, 73100 Lecce, Italy
Muhammad Khalid: Center for Biomolecular Nanotechnologies, Istituto Italiano di Tecnologia, Via Barsanti, 73010 Arnesano, Italy
Fabio Della Sala: Center for Biomolecular Nanotechnologies, Istituto Italiano di Tecnologia, Via Barsanti, 73010 Arnesano, Italy; and Institute for Microelectronics and Microsystems (IMM-CNR), Via Monteroni, Campus Unisalento, 73100 Lecce, Italy

purely local interaction, i.e. $\varepsilon(\mathbf{r}, \mathbf{r}'; \omega) \simeq \varepsilon(\mathbf{r}, \omega)\delta(\mathbf{r}-\mathbf{r}')$. At few-nanometer length scales, however, this local response approximation (LRA) breaks down, and nonlocal corrections must be considered. The simplest corrections beyond the LRA are obtained by including the Thomas-Fermi (TF) electron pressure into a hydrodynamic-like description of the free-electron gas [37]. In this approximation, the equilibrium density is often assumed to be a constant and boundary conditions are imposed in order to prevent the electron from escaping the metal surface (hard-wall boundary conditions).

Purely quantum effects, by contrast, typically require the density functional theory (DFT) formalism [38], which allows a description of the interaction of single electron states [39]. A time-dependent (TD) DFT has been recently used to explore electron tunneling in nonlinear nanoplasmonics [40, 41] and to study the impact of the atomistic nature of matter on plasmonic systems [42]. Methods based on DFT are, however, computationally very expensive and are limited to small clusters, although efforts to increase their range of applicability are continuously being made [43–46]. Yet, by definition, nanoplasmonics concerns (non-interacting) collective states. It is then reasonable to describe free-electrons in a metallic system by a single collective quantum-like state. This can be done through the quantum hydrodynamic theory (QHT) which accounts for density-gradient (∇n-dependent) correction to the total internal electron energy and spatially-dependent equilibrium charge densities [47–51]. The advantage of QHT is that it can be applied to large systems that are out-of-reach of DFT calculations. This theory has been very recently applied in a tunneling regime to investigate nonlocal and quantum effects, showing good agreement with TD-DFT calculations [52].

Quantum emitters are characterized by strong evanescent fields that quickly decay away from their close proximity. The closer they are to a nanoplasmonic system, the more efficiently their fields can probe nonlocal and quantum effects in the metal response [1–4]. Recent studies have highlighted the impact of nonlocality on single-emitter weak coupling [53–55], as well as in plasmon-exciton systems in the strong coupling regime [56]. Quantum effects have also been investigated in metals, in plasmon-exciton systems [57], and in molecules, beyond the point-dipole approximation [21].

In this article, we theoretically examine the dynamics of a single quantum emitter placed at nanometer and sub-nanometer distances from nanoplasmonic systems (Figure 1). We show that, at such distances, the hydrodynamic theory (even in the TF approximation) leads to a significant difference from the LRA. To account for quantum effects in the metal, we employ a state-of-the-art QHT [50], which allows the study of nonlocal, electron spill-out and quantum broadening effects. We find a significant qualitative deviation between models in the weak coupling regime that leads to quantitative differences in the strong coupling regime. In nano-gap systems, the inclusion of electron spill-out and quantum broadening leads to the existence of an optimal gap size for Rabi splitting that minimizes the requirements on the emitter oscillator strength. This is in contrast with LRA results where Rabi splitting increases indefinitely as the gap shrinks. Our analysis is performed on systems the size of which have experimental relevance. Finally, the impact of *d*-band electrons in noble metals is examined.

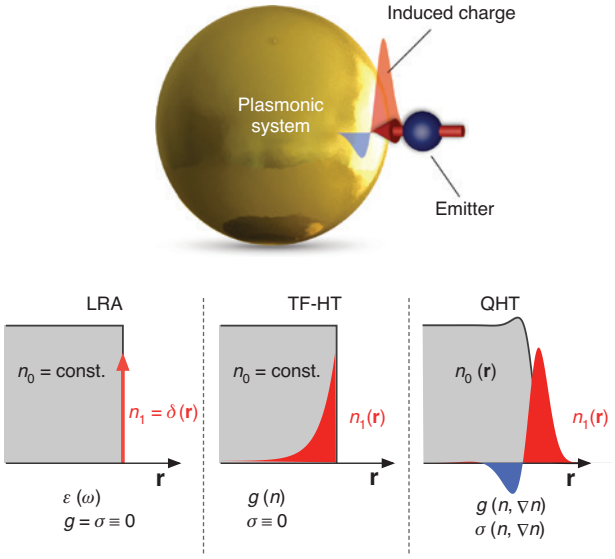

Figure 1: Schematic of a close interaction of an emitter with the induced electron density in the metallic system.
On the bottom is a summary of the three different response models. In the local response approximation (LRA), the induced charge density is a Dirac delta function centered at the metal surface; in the Thomas-Fermi hydrodynamic theory (TF-HT), electrons accumulate near the metal surface without being able to escape; in the quantum hydrodynamic theory (QHT) the equilibrium density is exponentially decaying across the metal surface and the induced charges are smeared both inside and outside the metal-air interface.

2 Results and discussion

2.1 Theoretical framework

In a general hydrodynamic description, the linear nonlocal relation of the polarization vector $\mathbf{P}(\mathbf{r}, \omega)$ and the electric field $\mathbf{E}(\mathbf{r}, \omega)$ is described by the equation [47–50]:

$$-\frac{en_0}{m}\nabla g(n,\nabla n)+\frac{e}{m}\nabla\cdot\sigma(n,\nabla n,\omega)-(\omega^2+i\gamma\omega)\mathbf{P}=\varepsilon_0\omega_p^2\mathbf{E}, \quad (1)$$

where e and m are, respectively, the magnitude of the charge and the mass of the electron, $n(\mathbf{r},\omega)=n_0(\mathbf{r})+\frac{1}{e}\nabla\cdot\mathbf{P}$ is the electron density with n_0 being the equilibrium charge density, γ is the phenomenological damping rate and $\omega_p(n_0)$ is the plasma frequency. The first term in Eq. (1) takes into account electron-electron interactions and represents the quantum pressure. In particular, g is the first-order term (with respect to perturbations of n) of the functional derivative of the energy functional G, i.e. $g=\left(\frac{\delta G[n]}{\delta n}\right)_1$. The complexity of the energy functional sets the level of approximation of the QHT. In this article we will take $G[n]$ as the sum of the TF kinetic energy functional, the von Weizsäcker (vW) correction and the exchange-correlation (XC) energy term in the limit of the local density approximation, i.e. $G[n,\nabla n]=T_{TF}[n]+T_{vW}[n,\nabla n]+E_{XC}[n]$. The second term in Eq. (1) has the form of a viscoelastic tensor and takes into account the nonlocal damping [58, 59], which is especially relevant for geometries with small features [50]. Explicit expressions for these functionals can be found in Refs. [49] and [50].

If we set both $g=\sigma\equiv 0$, Eq. (1) reduces to the usual Drude model in which the relation between E and P is purely local. We will refer to this approximation as LRA. In the TF hydrodynamic theory (TF-HT) only the TF kinetic energy functional is considered, i.e. $G[n]=T_{TF}$. In this approximation we will also set $\sigma=0$ and $n_0=$ constant in the metal volume throughout the article. The principal characteristics for each approach are summarized in Figure 1.

Coupled to the continuity equation and Maxwell's equations, Eq. (1) describes the optical response of metals. In its general form it takes into account nonlocal electron response, electron charge spill-out, size-dependent absorption and retardation effects. We have implemented this system of equations in a finite-element method (FEM) commercial platform using a 2.5D scheme [49, 50, 60] for axis symmetric structures. The single-molecule emission is approximated by a point-like dipole field and its interaction with the plasmonic system is implemented using a scattering field formulation that avoids numerical complications due to the singularity of the dipole field (see the Methods section for more details).

In order to study the strong interaction of the emitter with the metallic system described by Eq. (1) we employ the method developed by Alpeggiani et al. [61], which allows the study of non-perturbative effects by evaluating the perturbative photon emission decay rate. In this framework, the power spectrum (averaged over the solid angle) emitted to the far-field by a point-like dipole in proximity to a metal nanostructure is given by [61, 62]:

$$S(\omega)=\frac{\hbar\omega}{2\pi}q(\omega)\gamma_{tot}(\omega)S'(\omega). \quad (2)$$

where the dipole spectrum S' is defined as:

$$S'(\omega)=\left|\frac{1}{i[\omega_0-\omega-\delta\omega(\omega)]+\frac{1}{2}\gamma_{tot}}\right|^2, \quad (3)$$

where ω and ω_0 are, respectively, the emitted frequency and the dipole transition frequency, $\gamma_{tot}=\gamma_r+\gamma_{nr}$ is the perturbative dipole decay rate (including radiative and non-radiative contributions), $\delta\omega$ the photonic (anomalous) Lamb shift, and $q=\gamma_r/\gamma_{tot}$ is the quantum yield of the system, which gives the probability that a transition of the emitter results in photon emission to the far-field as opposed to being absorbed by the nearby environment.

$S(\omega)$ is the energy radiated by the dipole at frequency ω. Since no external excitation is present in our system, $S(\omega)$ represents the number of photons of energy $\hbar\omega$ emitted in the far-field per unit of time in all directions. Evaluating this quantity corresponds to measuring luminescence in experimental setups. The quantity $S'(\omega)$, by contrast, represents the total number of photons emitted by the molecule, including those that are lost (absorbed) in the plasmonic environment and do not reach the far-field.

All the quantities introduced can be calculated from the electromagnetic fields as detailed in the Methods section.

2.2 Spheres

Before delving into the strong coupling regime calculations, it is interesting to observe the impact of nonlocal and quantum effects on near-field and far-field optical properties by comparing the electromagnetic local density of states (LDOS) $\rho(\mathbf{r}_0,\omega)$ and the extinction spectra, respectively. In the following, we normalize the extinction cross-section to the geometric cross-section (πR^2 for spheres and $2\pi R^2$ for sphere dimers), which yields the extinction efficiency q_{ext}. Similarly, we normalize the LDOS to the free-space LDOS, $\rho_0(\omega)=\omega^2/(\pi^2c^3)$. Moreover, since the dipole parallel component is quenched at very small distances from metal surfaces [63], we only consider a dipole normally oriented with respect to the close-by metal surface.

Figure 2 depicts the extinction efficiency and the LDOS enhancement spectra for Drude-like Na spheres of radius R varying from 2.5 nm to 20 nm. The LDOS refers to the states that can be excited by a point-like dipole placed at $d=1$ nm from the nanoparticle, normally oriented (as shown in the inset of Figure 2B). The QHT results are compared against the LRA and the TF-HT calculations. It is interesting to notice that for the smallest particle ($R=2.5$ nm) both the extinction and the LDOS are strongly affected by the model used to describe the metal particle. The LRA extinction shows the usual dipole resonance at $\omega=\omega_p/\sqrt{3}$, which appears shifted toward the blue in the TF-HT spectra and toward the red in the QHT spectra [48]. The TF-HT shows a set of resonances above the plasma frequency due to longitudinal modes [37]. These modes are not visible in the QHT spectra, due to additional nonlocal losses introduced by the viscoelastic tensor [50], which visibly broadens the dipole resonance. As the particle size increases, the extinction spectra for the different models converge to the same curve, as would be expected. Surprisingly, this is not the case for the LDOS spectra, which remain neatly different even for the largest nanoparticle ($R=20$ nm). The LRA spectra show a set of new resonances in addition to the dipole resonance that tend to sum up into a large *super-resonance* peak around $\omega=\omega_p/\sqrt{2}$ for bigger particles. Note that this is the surface plasmon resonance condition for a flat surface. The limit of a dipole infinitesimally close to the sphere is, in fact, equivalent to a dipole nearby an infinitely large sphere. The TF-HT, however, displays resonances above the LRA limit $\omega_p/\sqrt{2}$, as already pointed out by Christensen and co-authors [54]. More interesting is the fact that as the particle size is increased, the TF-HT spectrum seems to build up similarly to the LRA case, although this time into a much broader resonance above $\omega_p/\sqrt{2}$. For the QHT spectra, with respect to the extinction, everything is blurred by the presence of nonlocal losses, which are always large due to the fact that the dipole is extremely close to the metal surfaces. Although broad, a resonance can be seen converging below $\omega_p/\sqrt{2}$ for larger distances. Similar results have been recently observed by Gonçalves et al. [64] using the Feibelman d-parameters approach, in which the surface

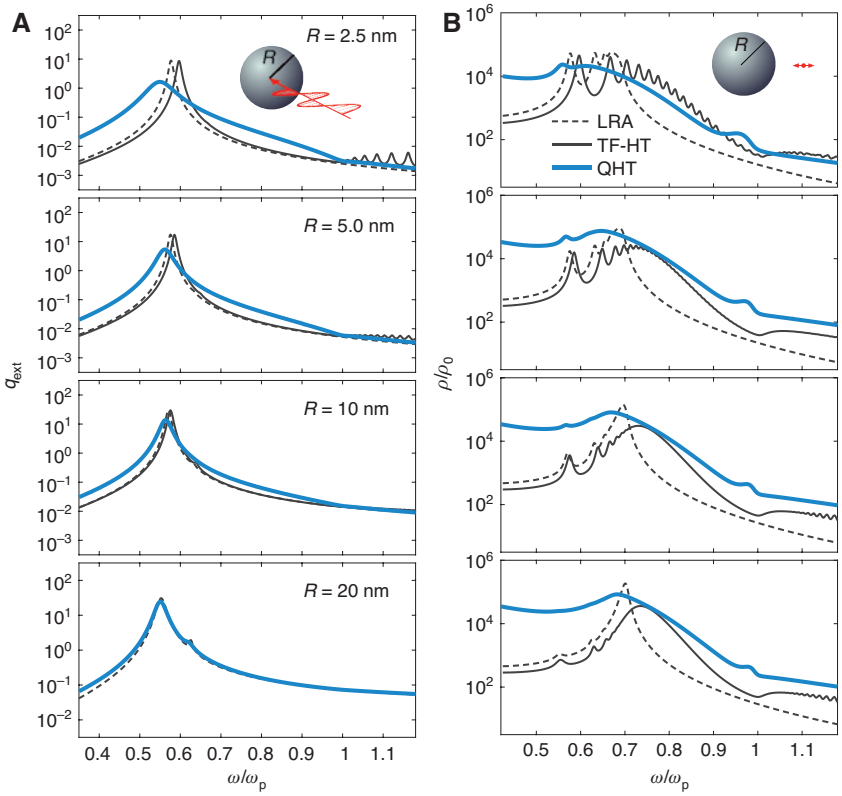

Figure 2: Far-field versus near-field properties for metallic spheres of different radii R, for the local response approximation (LRA), Thomas-Fermi hydrodynamic theory (TF-HT) and quantum hydrodynamic theory (QHT) models, respectively.
(A) The extinction efficiency spectra. (B) The normalized local density of states (LDOS) for states excited by a normally oriented dipole placed at a fixed distance $d=1$ nm. In our calculations we assumed a Drude-like metal with bulk parameters $\hbar\omega_p=5.89$ eV and $\hbar\gamma=0.066$ eV corresponding to sodium (Na).

effects are embedded in an effective frequency-dependent parameter. The QHT, however, goes beyond purely surface effects and offers a full nonlocal (**k**-dependent) description of the free-electron dynamics, which is particularly relevant when the emitter is in very close proximity to the metal surface. In the QHT spectra, a new resonance can be seen right below the bulk plasma frequency ω_p, persisting even for the largest particle. It is, however, hard to identify the nature of the mode in question since the field maps are mostly characterized by the strong evanescent fields of the dipole.

Next, we fix the particle radius at $R=20$ nm and we vary the distance d of the emitter from the nanoparticle. Figure 3 shows the spontaneous (total) and radiative emission rate enhancement, γ_{tot}/γ_0 and γ_r/γ_0, respectively, for all considered models. As expected, at large distances ($d=16$ nm), all models converge to an identical spectrum, in which the dipole resonance is clearly distinguishable from higher order modes. As the distance is reduced, we obtain, for the total rate, similar results as for the LDOS in Figure 2 for the largest particles. Interestingly, the radiative decay rate enhancement remains similar for all distances, throughout the different models. This is not unexpected since γ_r takes into account only those modes that radiate to the far-field. It is worth noting in all the spectra the presence of an antiresonance associated to a minimum in the radiative emission rate. This antiresonance behavior corresponds to the situation in which the induced dipole moment has an equal amplitude and opposite phase to the emitting dipole, resulting in an almost-zero radiation to the far-field.

This can be easily seen in the dipole-dipole approximation where the radiative decay rate enhancement reduces to [65]:

$$\frac{\gamma_r}{\gamma_0}=\left|1+\frac{2(\varepsilon-1)}{\varepsilon+2}\left(\frac{R}{R+d}\right)^6\right|^2. \tag{4}$$

Assuming a Drude-like dielectric constant for the nanoparticle, i.e. $\varepsilon=1-\frac{\omega_p^2}{\omega^2+i\gamma\omega}$, we obtain the following antiresonance condition:

$$\omega_{ar}=\sqrt{\frac{\omega_p^2}{3}\left(\frac{3+(d/R)^3}{1+(d/R)^3}\right)}+O(\gamma^2). \tag{5}$$

As the distance $d\to 0$, the antiresonance $\omega_{ar}\to\omega_p$. At frequency ω_{ar}, the radiative decay rate enhancement is minimum and its value is:

$$\left.\frac{\gamma_r}{\gamma_0}\right|_{min}=\frac{3}{4}(1+d/R)^3\left[2+(1+d/R)^3\right]\left(\frac{\gamma}{\omega_p}\right)^2+O(\gamma^4). \tag{6}$$

From Eq. (6) it can be seen that the minimum value decreases monotonically with d. This is quite evident in Figure 3 for the LRA and TF-HF, but it is not the case for the QHT, where $\left.\frac{\gamma_r}{\gamma_0}\right|_{min}$ increases going from $d=2$ nm to 1 nm. This fact can be related to spill-out effects, where classical formulas break down. In Figure 4 we plot the equilibrium and induced charge densities, n_0 and n_1, respectively, along the z-axis as a function of the distance from the emitter for

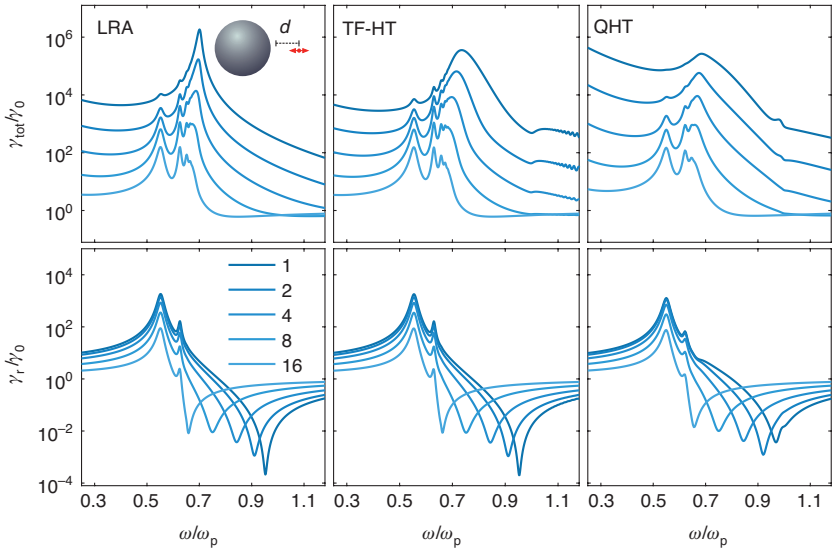

Figure 3: Normalized total and radiative decay rates for an emitter placed near a metallic sphere (as in Figure 2) with a fixed radius of $R=20$ nm; the emitter is normally oriented with respect to the metal surface and placed at distances d (shown in nanometers).

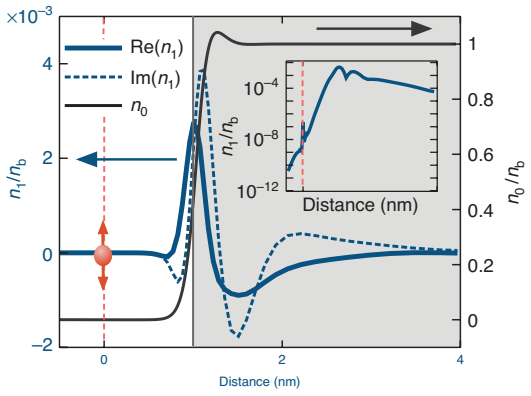

Figure 4: Equilibrium and induced charge densities, n_0 and n_1, respectively, along the z-axis as a function of the distance from the emitter calculated using the quantum hydrodynamic theory (QHT) at $\hbar\omega = 4$ eV.
The dipole emitter is shown in red. The shaded area represents the nanoparticle interior delimitated on the left by the ion edge. The inset shows the absolute value of the induced density in log scale.

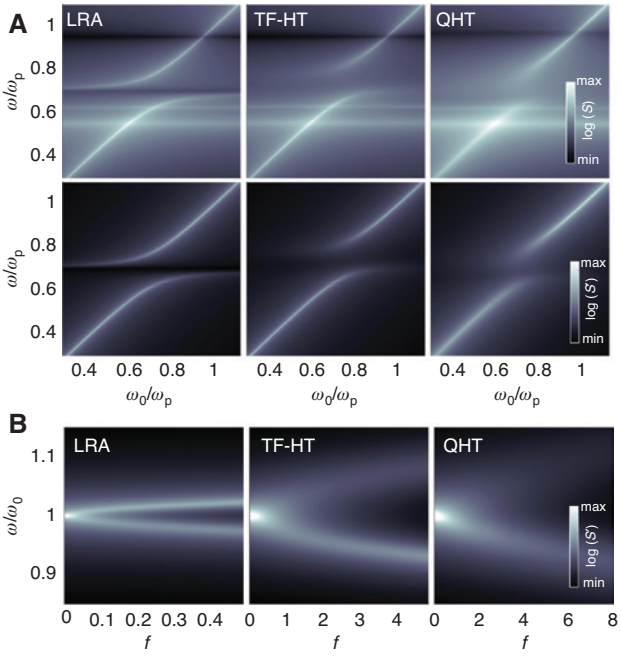

Figure 5: Fluorescent emission modification induced by a metallic nanosphere.
(A) Power and dipole strong coupling spectra as a function of the emitter frequency ω_0 for a dipole amplitude of $p = 25.7$ D. (B) Dipole spectra as a function of the oscillator strength f for a dipole placed at distance $d = 1$ nm from a metallic sphere. The emitter frequency is $\hbar\omega_0 = 4.13$ eV for the local response approximation (LRA), $\hbar\omega_0 = 4.33$ eV for the Thomas-Fermi hydrodynamic theory (TF-HT) and $\hbar\omega_0 = 4.00$ eV for the quantum hydrodynamic theory (QHT) calculations, respectively.

the QHT. Contrarily to the other models (LRA and TF-HT, for which there is no electron spill-out), in this case the emitter is overlapped with the electron density tail that decays exponentially away from the particle's ion edge.

It is worth pointing out that although exact electrodynamic solutions exist for both the LRA [66] and the TF-HT [54, 67] cases, their implementation involves infinite sums of higher-order multipoles. While higher-order multipole contribution to radiative rates is negligible, this is not the case for non-radiative rates [68], especially if small distances between the dipole and the metal surface are considered. The numerical evaluation of these large analytical sums may limit the minimum distance that can be practically computed to 1 nm. Our FEM implementation based on the scattering field formalism (see Methods section) allows calculation of the non-radiative decay rates also for sub-nanometer distances.

The quantities analyzed so far are independent (besides a scaling factor) from the dipole moment $\mathbf{p}$ of the molecule. The non-perturbative quantities defined in Eqs. (2) and (3), by contrast, strongly depend on these parameters. Figure 5A shows the power and dipole spectra (S and S', respectively) as a function of the emitter frequency ω_0 for a dipole moment of $p = |\mathbf{p}| = 25.7$ D. As the emitter frequency is swept, anti-crossing appears around the main peak in the total emission rate spectrum. Interestingly, this is a dark mode that can be clearly seen in the S maps as a dark horizontal line around $\omega = \omega_p/\sqrt{2}$. The possibility of strong coupling with dark modes was already pointed out by Delga et al. [69] where a collection of quantum emitters interacting with a metal nanoparticle was theoretically analyzed. In contrast, the dipolar and the quadrupolar modes appear as light horizontal lines, although they do not show any strong coupling. Another interesting feature clearly visible in the S maps of Figure 5A is the deep horizontal line associated to the antiresonance in the radiative decay rate spectra. Because this is a far-field effect, there is no strong interaction with the emitter. The strong coupling between the emitter and the nanoparticle is clearly visible for all models in the dipole spectrum S' maps (second row of Figure 5A).

The analysis of Rabi splitting is more easily done in terms of the dimensionless oscillator strength $f = \frac{2}{3}\frac{m\omega_0 p^2}{e^2\hbar}$ of the emitting dipole rather than the dipole moment. Figure 5B shows the dipole spectrum S' as a function of the oscillator strength for ω_0 tuned at the peak of γ_{tot}. From these maps it is possible to roughly identify the oscillator strength necessary to observe Rabi splitting, namely $f_{th}^{LRA} \simeq 0.05$, $f_{th}^{TF} \simeq 1$ and $f_{th}^{QHT} \simeq 2$. The oscillator strength threshold for the TF-HT and the QHT is more than one order of magnitude bigger than the LRA case. While this is somehow expected in the QHT case because of the

extra losses due to viscosity, it is a surprising result for the TF-HT. In fact, although similar systems have already been investigated by some of the authors of this article [70], this result has not been observed before. On the contrary, Tserkezis et al. [56, 71] have demonstrated robustness of strong coupling against nonlocal corrections, when collective emitters are considered. As we will see later, however, this behavior is hindered in the vicinity of noble metal systems, since photon emission spectra are strongly affected by *d*-band transitions.

2.3 Sphere dimers

Metallic structures that are characterized by few-nanometer or even sub-nanometer inter-particle distances achieve the largest optical field confinement [25, 29] and smallest optical cavity volumes, and are ideal candidates for achieving single-molecule room temperature strong coupling [56, 62, 70–72]. We consider dimers of Drude-like Na spheres of radius R and gap size $g = 2d$. As in the previous section, it is instructive to first analyze far-field against near-field properties. Figure 6 shows the extinction efficiency and normalized LDOS spectra for dimers characterized by a fixed gap $g = 2$ nm for different sphere radii. The extinction spectra refer to an incident plane wave the electric field of which is polarized along the dimer axis, and the LDOS spectra refer to the states that can be excited by a point-like dipole placed at the center of the gap and oriented along the dimer axis, as shown in the insets of Figure 6A and B, respectively. The QHT results are compared against the LRA and the TF-HT calculations. Contrarily to the single sphere of the previous section, in the dimer system, it is possible to clearly observe higher order resonances as R increases. As expected, the dipole resonance clearly shifts toward lower energies. In particular, in the LDOS spectra, the dipole resonance is always clearly distinguishable (for all models), even for the larger dimers, contrarily to what we observed for the single spheres. As we will show later, this allows a strong coupling of the molecule and the dipolar mode. Differences between the LRA, TF-HT and QHT are analogous to the single sphere case.

In Figure 7A we plot the spontaneous (total) and radiative emission rate enhancement for different gap sizes and a

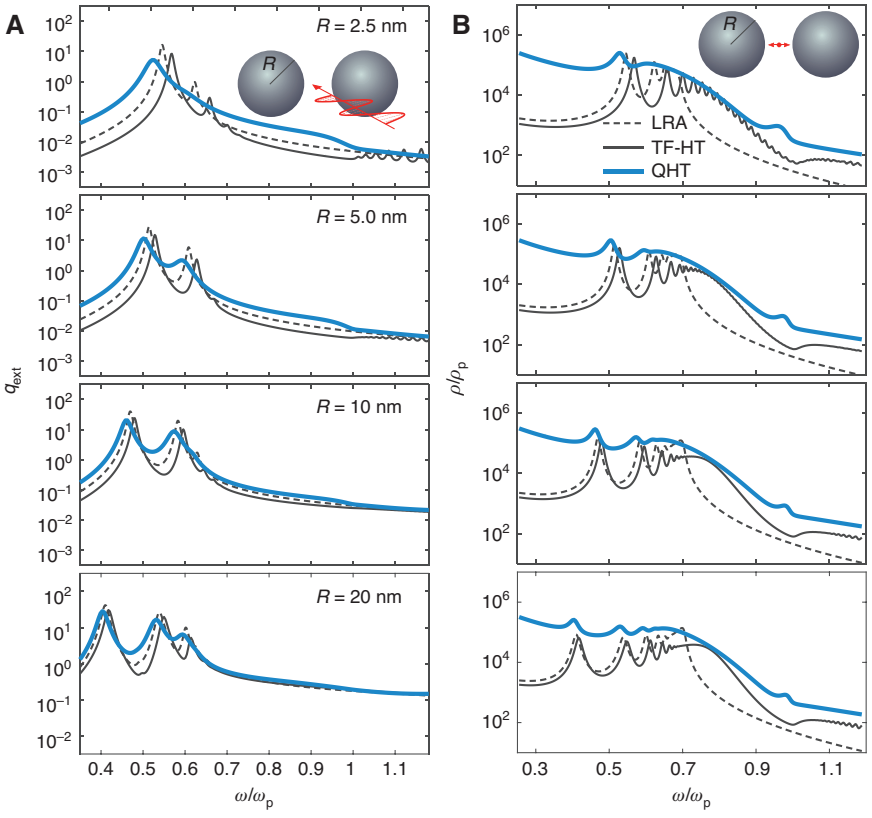

Figure 6: Far-field versus near-field properties for metallic dimers constituted by identical spheres of various radii R, for the local response approximation (LRA), Thomas-Fermi hydrodynamic theory (TF-HT) and quantum hydrodynamic theory (QHT) models, respectively. (A) The extinction efficiency spectra for a fixed gap size $g = 2$ nm. (B) The normalized local density of states (LDOS) for a dipole parallel to the dimer axis and placed at the center of the gap, i.e. $d = 1$ nm. Material parameters as in Figure 2.

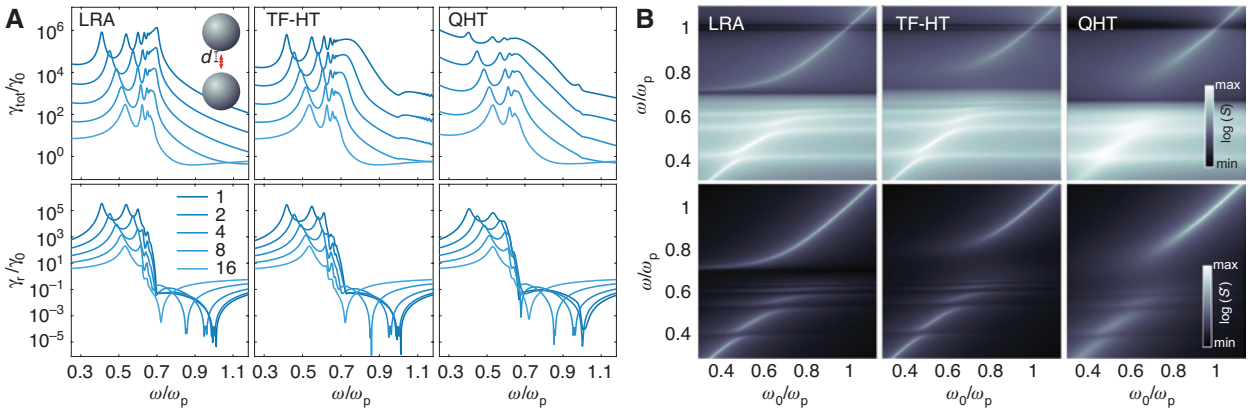

Figure 7: Emission properties of a single molecule placed at the center of a plasmonic dimer.
(A) Normalized total and radiative decay rates for an emitter placed at the center of a metallic sphere dimer as shown in the inset for a fixed radius of $R = 20$ nm; the emitter is parallel to the dimer axis and placed at distances $d = g/2$ (indicated in nanometers) from the particles.
(B) Power and dipole strong coupling spectra as a function of the emitter frequency ω_0 for a dipole amplitude of $p = 25.7$ D.

fixed particle radius for all considered models. Similarly to the single sphere case, at large gaps (and larger emitter distances), all models converge to the same spectrum for both γ_{tot} and γ_r. At such large gap sizes ($g = 32$ nm), nonlocal and quantum effects are indeed expected to be negligible. As the gap closes, differences between models start to emerge, although, they show qualitatively similar resonances below the plasma frequency. The total decay rate enhancement reaches similar peak values at the dipolar resonance, but it tends to increase at lower energies in the QHT spectra because of the stronger losses due to the viscosity term in Eq. (1). Also in this case, it is possible to identify the antiresonance behavior in the radiative emission rates, although no simple analytical formulas are known for dimers.

Let us now study the strong coupling regime. Figure 7B shows the power and dipole spectra as a function of the emitter frequency ω_0 for $g = 2d = 2$ nm and a molecule with a dipole moment of $p = 25.7$ D. As anticipated earlier, it is possible in this case to clearly see anti-crossing behavior around the dipolar mode as well other higher order radiative modes, on top of the coupling with the dark mode observed for the spheres. The dipole spectra as a function of the oscillator strength in Figure 8 show that all models predict a similar threshold $f_{th} \sim 0.5$ for a gap $g = 2$ nm (or $d = 1$ nm). For a smaller gap, $g = 1$ nm (or $d = 0.5$ nm), the oscillator strength threshold reduces to $f_{th} \sim 0.1$ for the LRA and TF-HT, while the QHT spectra become too broad to identify any threshold. Interestingly, when nonlocal broadening is considered, there appears to be an optimal gap distance for being able to observe strong coupling. Figure 9A shows the dipole spectrum for different values of the dimer gap size, i.e. the distance from the emitter. The LRA and the TF-HT predict a similar behavior: as the

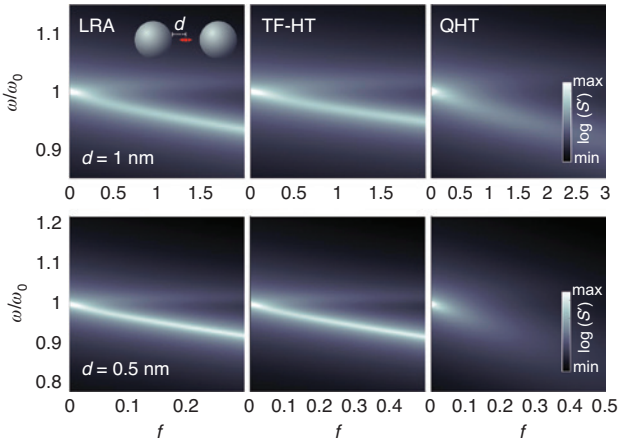

Figure 8: Dipole spectra as a function of the oscillator strength f for a dipole placed at the center of the sphere dimer.
In (A) $g = 2d = 2$ nm and the emitter frequency is $\hbar\omega_0 = 2.42$ eV for local response approximation (LRA), $\hbar\omega_0 = 2.46$ eV for Thomas-Fermi hydrodynamic theory (TF-HT), and $\hbar\omega_0 = 2.38$ eV for quantum hydrodynamic theory (QHT) calculations, respectively. In (B) $g = 2d = 1$ nm and the emitter frequency is $\hbar\omega_0 = 2.15$ eV for LRA, $\hbar\omega_0 = 2.22$ eV for TF-HT, and $\hbar\omega_0 = 2.08$ eV for QHT calculations, respectively.

gap shrinks, the coupling strength increases generating a Rabi splitting that increases indefinitely. In the case of the QHT, the Rabi splitting appears for a sufficiently large coupling but disappears for the smallest gap size, as mentioned above. This peculiar behavior is due to the increase of losses as the emitter overlaps with the electron density tail, as shown in Figure 9B. This is clearly visible in the log-scale plot, where the self-consistent QHT density accounts for a non-zero charge density value in the gap region.

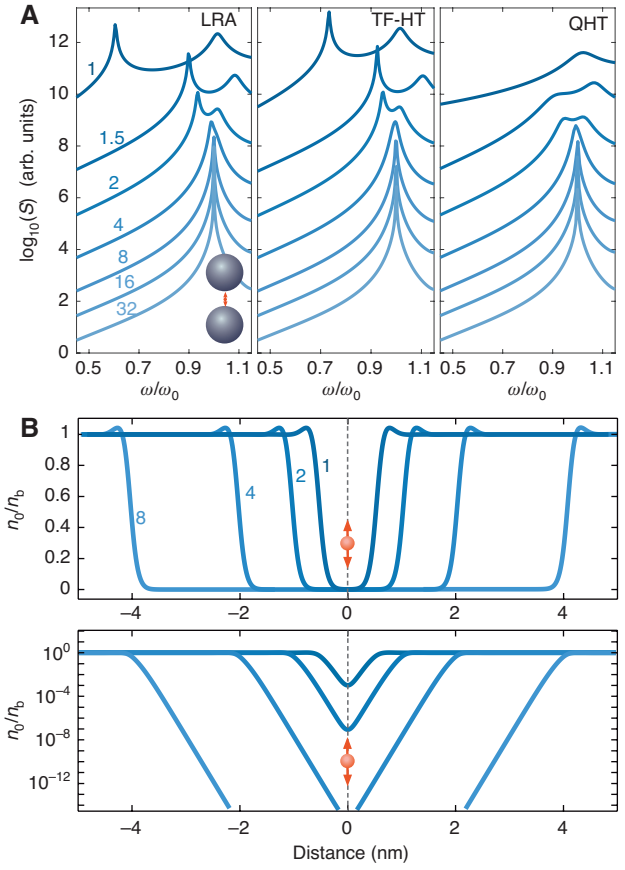

Figure 9: Influence of the electron density tail on the emission properties.
(A) Dipole spectra for different dimer gap sizes and fixed oscillator strength $f=2$. The oscillator frequency ω_0 is as in Figure 8 for the different models. In (B) the equilibrium electron density is along the dimer axis in the linear (top) and log (bottom) scale. The emitter position is depicted in red.

Although in this work we approximate the emitter as a point-dipole source, in this overlap regime, the effects due to the finite size [21, 73] of the light source might not be negligible, and would require a more sophisticated description of the emitter. One possibility would be to use the QHT to describe both the metal structure and the emitter. In this case, the charge transfer between the emitter and the structure and the nonlocality of the emitter would also be considered.

2.4 Gold structures

So far we have considered Drude-like metal nanoparticles and even if we considered parameters for sodium, our previous results still remain nearly ideal. Although this was useful to understand the underlying behavior of the systems, it is also important to characterize the impact of more practical materials. Any plasmonic experiment is in fact performed using noble metal nanoparticles.

Figure 10A shows decay rate enhancements for a gold sphere dimer characterized by a gap $g=2$ nm. The spectra are clearly affected by the larger losses due to interband transitions. This also strongly impacts the strong coupling regime as shown in Figure 10B and C. We cannot distinguish an anti-crossing or a Rabi splitting behavior. Instead, as we increase the dipole strength (Figure 10C) we can only observe a shift of the emitter frequency towards lower energies. This is due to the dielectric component ($\varepsilon_{\text{core}}$) of the gold permittivity in the high-end part of the visible spectrum.

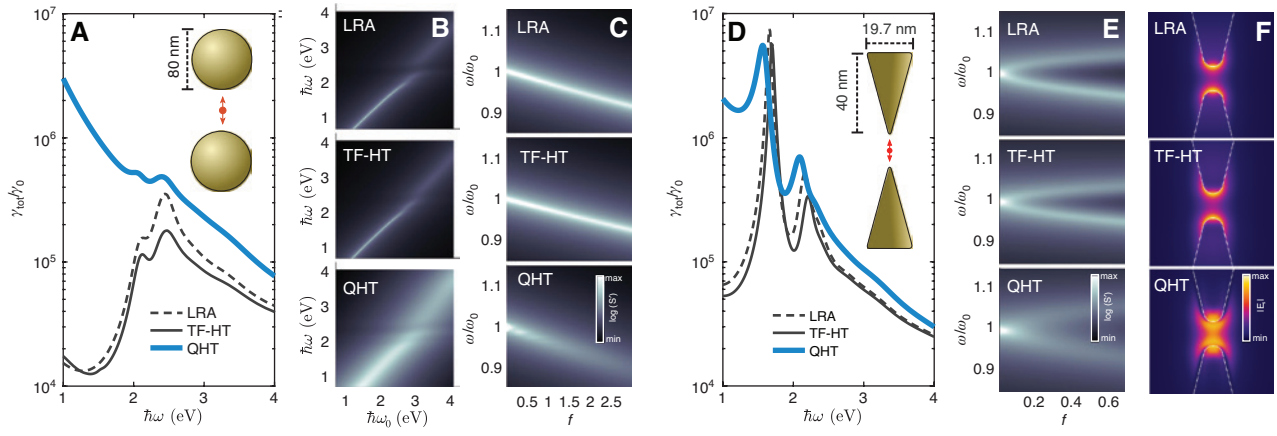

Figure 10: Emission properties of a dipole emitting near the gold systems shown in the insets, for a gap $g=2$ nm for different models.
(A) Total decay rates and (B) dipole spectra as a function of the emitter frequency ω_0 and the oscillator strength f (C) for a sphere dimer. Total decay rates (D), dipole spectra as a function of the oscillator strength f and local scattering field map (E) for a cone dimer.

In order to avoid this issue, we consider a dimer constituted by two sharp tips or cones, as depicted in the inset of Figure 10D. We limit, however, the sharpness of the structure to a radius of curvature of the tip of $r_{tip} = 0.4$ nm. The cone dimer allows the dipolar resonance to shift towards lower energies, increase its strength and at the same time reduce the mode volume. These properties allow observation of a Rabi splitting for oscillator strength of the order of $f_{th} \sim 0.1$ for the LRA and TF-HT and $f_{th} \sim 0.2$ for the QHT, as shown in Figure 10E. Figure 10F shows the norm of the scattered field $|\mathbf{E}_s| = |\mathbf{E} - \mathbf{E}_{dipole}|$, $\mathbf{E}_{dipole}$ being the electric field associated to the dipole. The impact of the electron density spill-out is clearly visible for the QHT maps.

Although the impact of *d*-band electrons is detrimental for observing strong coupling, atomistic features [42, 74] in real systems might provide some extra field confinement, allowing strong coupling observation in real systems [72]. Another important role could be played by the spatial extension of real molecules [21], which goes beyond the point dipole approximation used in this work.

3 Conclusions

In this paper we have investigated the impact of nonlocal and quantum effects on the strong coupling of a single emitter placed in extremely close proximity to plasmonic nanostructures. At such distances, when non-radiative modes become predominant, the hydrodynamic theories lead to a significant deviation from LRA calculations. We have shown that strong coupling with dark modes in metallic spheres can lead to an increase of the oscillator strength threshold at which Rabi splitting can occur by about one order of magnitude if nonlocal and quantum effects are considered. This suggests that it might be possible to observe single-molecule strong coupling by properly engineering doped semiconductor nanoparticles in order to reduce the impact of nonlocal and quantum effects at lower frequencies. By considering nano-gap plasmonic sphere dimers, we show that it is, in principle, possible to realize strong coupling of molecules with radiative plasmonic modes and observe Rabi splitting for realistic oscillator strengths ($f \simeq 0.5$). Quantitative and qualitative differences are predicted when quantum effects are considered. Electron spill-out and quantum broadening limit the minimum gap size that can be used to observe Rabi splitting. We also performed calculations for gold systems and showed that *d*-band electrons could be very detrimental to the observation of strong coupling. Nonetheless, resonance splitting in the extinction spectra [72] and fluorescence spectra [75] has been observed experimentally. It is worth pointing out that our calculations still predict strong coupling interactions (i.e. a shift of the dipole frequency) in gold structures, although a clear observation of Rabi splitting is hindered. As mentioned above, this could be, however, circumvented by properly engineering specific geometrical features that reduce the mode volume or shift the plasmonic modes toward lower frequencies.

Moreover, while we have employed a sophisticated method to describe the plasmonic environment, we have still considered the molecule in the point-dipole approximation. It is not excluded then that in very close proximity of the metal surface, where strong field gradients occur, the nonlocal nature and spatial extension of the emitting molecule could become very important. This problem could be solved in the near future by using the QHT to describe the emitter as an extended quantum-dot rather than an ideal point-dipole.

4 Methods

The total spontaneous emission rate γ_{tot} for an emitter located at position $\mathbf{r}_0$ can be calculated from Fermi's Golden Rule as [63, 76]:

$$\gamma_{tot}(\mathbf{r}_0, \omega) = \frac{\pi\omega}{3\hbar\varepsilon_0} |\mathbf{p}|^2 \rho(\mathbf{r}_0, \omega), \tag{7}$$

where $\mathbf{p}$ is the dipole transition moment and ρ is the electromagnetic LDOS. We can express the LDOS using the system's dyadic Green's function, $\mathbf{G}$ as:

$$\rho(\mathbf{r}, \omega) = \frac{6\omega}{\pi c^2} [\hat{\mathbf{n}}_p \cdot \mathrm{Im}\{\mathbf{G}(\mathbf{r}, \mathbf{r})\} \cdot \hat{\mathbf{n}}_p], \tag{8}$$

where $\hat{\mathbf{n}}_p$ is the dipole moment unit vector. Analogously, the Lamb shift can be calculated by [77]:

$$\delta\omega(\mathbf{r}_0, \omega) = \frac{1}{\pi\hbar\varepsilon_0 c^2} \mathrm{P} \int_0^\infty \frac{\omega'^2}{\omega' - \omega} |\mathbf{p}|^2 [\hat{\mathbf{n}}_p \cdot \mathrm{Im}\{\mathbf{G}_{sc}(\mathbf{r}_0, \mathbf{r}_0)\} \cdot \hat{\mathbf{n}}_p] d\omega', \tag{9}$$

where P denotes the Cauchy principal value and $\mathbf{G}_{sc}$ is the scattering part of the Green function obtained by decomposing it as $\mathbf{G} = \mathbf{G}_0 + \mathbf{G}_{sc}$, $\mathbf{G}_0$ being its value in free space. The Lamb shift expression can be simplified if the lower bound of integration is extended to $-\infty$ which allows the application of the Kramers-Kronig relation [62]:

$$\delta\omega(\mathbf{r}_0, \omega) \simeq \frac{\omega^2}{\hbar\varepsilon_0 c^2} |\mathbf{p}|^2 [\hat{\mathbf{n}}_p \cdot \mathrm{Re}\{\mathbf{G}_{sc}(\mathbf{r}_0, \mathbf{r}_0)\} \cdot \hat{\mathbf{n}}_p]. \tag{10}$$

In our computational framework, the dyadic Green function can be calculated from the field scattered back by the *environment* to the dipole as:

$$\mathbf{E}(\mathbf{r}, \omega) = \mu_0 \omega^2 \mathbf{G}(\mathbf{r}, \mathbf{r}_0) \cdot \mathbf{p}_c, \tag{11}$$

where μ_0 is the permeability of free space (we assumed the relative permeability of the medium to be 1) and $\mathbf{p}_c$ is the classical dipole moment (not to be confused with the dipole transition moment $\mathbf{p} = \mathbf{p}_c/2$). The electric field $\mathbf{E} = \mathbf{E}_s + \mathbf{E}_i$ is obtained in the scattering field formulation by solving the following equations:

$$\begin{aligned} &\nabla \times \nabla \times \mathbf{E}_s - \frac{\omega^2}{c^2}\left(\mathbf{E}_s - \frac{1}{\varepsilon_0}\mathbf{P}\right) = 0 \\ &-\frac{en_0}{m}\nabla g + \frac{e}{m}\nabla \cdot \sigma - (\omega^2 + i\gamma\omega)\mathbf{P} = \varepsilon_0 \omega_p^2 (\mathbf{E}_s + \mathbf{E}_i), \end{aligned} \tag{12}$$

with $\mathbf{E}_s$ being the scattered field and $\mathbf{E}_i$ the z-oriented dipole field [70]:

$$\begin{aligned} \mathbf{E}_i = \frac{|\mathbf{p}_c|}{4\pi\varepsilon_0} \Bigg\{ &\left[\left(-\frac{k_0^2}{r} - \frac{3ik_0}{r^2} + \frac{3}{r^3}\right)\cos(\theta)\sin(\theta)\right]\hat{\rho} \\ &+ \left[\frac{k_0^2 \sin^2(\theta)}{r} + (3\cos^2(\theta) - 1)\left(-\frac{ik_0}{r^2} + \frac{1}{r^3}\right)\right]\hat{z}\Bigg\} e^{ik_0 r}, \end{aligned} \tag{13}$$

where $k_0 = \omega/c$, $r = \sqrt{\rho^2 + z^2}$ and $\theta = \arctan(\rho/z)$ with ρ being the radial cylindrical coordinate.

From the electromagnetic fields, it is possible to obtain the radiative component of the decay rate by integrating the power flowing out of the system:

$$\gamma_r = \frac{1}{2}\frac{\gamma_0}{W_0}\int_{\partial\Omega} \mathrm{Re}\{\mathbf{E} \times \mathbf{H}^*\} da, \tag{14}$$

where $\gamma_0 = \omega^3 |\mathbf{p}|^2 / 3\hbar\pi\varepsilon_0 c^3$ is the decay rate in free space and $W_0 = \omega^4 |\mathbf{p}_c|^2 / 12\pi\varepsilon_0 c^3$ the power radiated in free space by the dipole $\mathbf{p}_c$.

We solve Eq. (12) for axis-symmetric structures by expanding the fields as sums of cylindrical harmonics, that is to say with azimuthal dependence of the form $e^{im\varphi}$. This results in a set of two-dimensional equations that can be solved independently for each value of the azimuthal number m.

In the special case of a dipole oriented along z, which corresponds to the axis of symmetry of the geometry, only the term corresponding to $m = 0$ gives a non-zero contribution. Therefore, the whole three-dimensional problem can be reduced to a single two-dimensional problem that greatly reduces the numerical cost of the simulations.

For QHT calculations, we assume a jellium approximation [78, 79] in which electrons are confined by a uniform background positive charge $n^+ = (r_s^3 4\pi/3)^{-1}$, r_s being the Wigner-Seitz radius that is $r_s = 3\ a_0$ for Au and $r_s = 4\ a_0$ for Na. We compute the equilibrium electron density self-consistently by using the following nonlinear differential equation [50–52]:

$$\nabla \cdot \varepsilon(\mathbf{r}) \nabla \left(\frac{\partial G[n]}{\partial n}\right)_{n=n_0} + e^2(n_0 - n^+) = 0, \tag{15}$$

where ε is the spatially dependent permittivity. Equation (15) is obtained by combining the zeroth order QHT equation and the Poisson equation for the electrostatic potential [50]. The space-dependence of the ground-state density $n_0(\mathbf{r})$ is crucial in characterizing the optical response of nanoplasmonic systems.

In order to describe gold structures, the empirical frequency-dependent permittivity for single crystal gold measured in Ref. [80] was used for LRA calculations. For the hydrodynamic models (TF-HT and QHT), we assumed, on top of the free-electron response, a local response from core electrons: $\varepsilon_{\mathrm{core}}(\omega) = \varepsilon_{\mathrm{Olmon}}(\omega) - \chi_f(\omega)$, where $\chi_f = -\dfrac{\omega_p^2}{\omega^2 + i\gamma\omega}$ ($\hbar\omega_p = 8.614$ eV and $\hbar\gamma = 0.042$ eV), while the free-electron response was calculated using Eq. (1). The gold equilibrium density $n_0(\mathbf{r})$ for QHT was calculated assuming a background constant permittivity $\varepsilon_\infty = 8$.

References

[1] Vielma J, Leung PT. Nonlocal optical effects on the fluorescence and decay rates for admolecules at a metallic nanoparticle. J Chem Phys 2007;126:194704–8.

[2] Dvoynenko MM, Wang J-K. Revisiting strong coupling between a single molecule and surface plasmons. Opt Lett 2013;38:760–2.

[3] Huck C, Vogt J, Neuman T, et al. Strong coupling between phonon-polaritons and plasmonic nanorods. Opt Express 2016;24:25528–39.

[4] Dvoynenko MM. Fluorescence of molecules placed near a spherical particle: rabi splitting. Semicond Phys, Quantum Electron Optoelectron 2017;20:458–64.

[5] Kongsuwan N, Demetriadou A, Chikkaraddy R, et al. Suppressed quenching and strong-coupling of purcell-enhanced single-molecule emission in plasmonic nanocavities. ACS Photonics 2018;5:186–91.

[6] Li R-Q, Garca-Vidal FJ, Fernandez-Dominguez AI. Plasmon-exciton coupling in symmetry-broken nanocavities. ACS Photonics 2017;5:177–85.

[7] Kaminska I, Vietz C, Cuartero-González Á, et al. Strong plasmonic enhancement of single molecule photostability in silver dimer optical antennas. Nanophotonics 2018;7:643–9.

[8] Cuartero-González A, Fernández-Domnguez AI. Light-forbidden transitions in plasmon-emitter interactions beyond the weak coupling regime. ACS Photonics 2018;5:3415–20.
[9] Monroe C. Quantum information processing with atoms and photons. Nature 2002;416:238–46.
[10] Chang DE, Sørensen AS, Hemmer PR, Lukin MD. Quantum optics with surface plasmons. Phys Rev Lett 2006;97: 053002–4.
[11] Stuart DA, Haes AJ, Yonzon CR, Hicks EM, Van Duyne RP. Biological applications of localised surface plasmonic phenomenae. IEE Proc: Nanobiotechnol 2005;152:13–20.
[12] Yin Y, Alivisatos AP. Colloidal nanocrystal synthesis and the organic–inorganic interface. Nature 2005;437:664–70.
[13] Liu X. Strong light-matter coupling in two-dimensional atomic crystals. Nat Photon 2014;9:30–4.
[14] Fedutik Y, Temnov VV, Schöps O, Woggon U, Artemyev MV. Exciton-plasmon-photon conversion in plasmonic nanostructures. Phys Rev Lett 2007;99:136802–4.
[15] Savasta S, Saija R, Ridolfo A, Di Stefano O, Denti P, Borghese F. Nanopolaritons: vacuum Rabi splitting with a single quantum dot in the center of a dimer nanoantenna. ACS Nano 2010;4:6369–76.
[16] Novotny L. Strong coupling, energy splitting, and level crossings: a classical perspective. Am J Phys 2010;78:1199–4.
[17] Schlather AE, Large N, Urban AS, Nordlander P, Halas NJ. Near-field mediated plexcitonic coupling and giant Rabi splitting in individual metallic dimers. Nano Lett 2013;13:3281–6.
[18] Törmä P, Barnes WL. Strong coupling between surface plasmon polaritons and emitters: a review. Rep Prog Phys 2014;78:013901–35.
[19] Lalanne P, Yan W, Vynck K, Sauvan C, Hugonin J-P. Light interaction with photonic and plasmonic resonances. Laser Photonics Rev 2018;12:1700113–38.
[20] Yoo D, Nguyen N-C, Moreno LM, et al. High-throughput fabrication of resonant metamaterials with ultrasmall coaxial apertures via atomic layer lithography. Nano Lett 2016;16:2040–6.
[21] Neuman T, Esteban R, Casanova D, Garca-Vidal FJ, Aizpurua J. Coupling of molecular emitters and plasmonic cavities beyond the point-dipole approximation. Nano Lett 2018;18:2358–64.
[22] Roller E-M, Argyropoulos C, Högele A, Liedl T, Pilo-Pais M. Plasmon–exciton coupling using DNA templates. Nano Lett 2016;16:5962–6.
[23] Mertens J, Eiden AL, Sigle DO, Huang F. Controlling subnanometer gaps in plasmonic dimers using graphene. Nano Lett 2013;13:5033–8.
[24] Fernández-Domnguez AI, Bozhevolnyi SI, Mortensen NA. Plasmon-enhanced generation of nonclassical light. ACS Photonics 2018;5:3447–51.
[25] Romero I, Aizpurua J, Bryant GW, Garca de Abajo FJ. Plasmons in nearly touching metallic nanoparticles: singular response in the limit of touching dimers. Opt Express 2006;14:9988.
[26] Fernández-Domnguez AI, Maier SA, Pendry JB. Transformation optics description of touching metal nanospheres. Phys Rev B 2012;85:165148.
[27] Aubry A, Lei D, Maier SA, Pendry J. Conformal transformation applied to plasmonics beyond the quasistatic limit. Phys Rev B 2010;82:205109.
[28] Kern J, Großmann S, Tarakina NV, Häckel T. Atomic-scale confinement of resonant optical fields. Nano Lett 2012;12:5504–9.
[29] Cirac C, Hill RT, Mock JJ, et al. Probing the ultimate limits of plasmonic enhancement. Science 2012;337:1072–4.
[30] Savage KJ, Hawkeye MM, Esteban R, Borisov AG, Aizpurua J, Baumberg JJ. Revealing the quantum regime in tunnelling plasmonics. Nature 2012;491:574–7.
[31] Raza S, Stenger N, Kadkhodazadeh S, et al. Blueshift of the surface plasmon resonance in silver nanoparticles studied with EELS. Nanophotonics 2013;2:131–8.
[32] Scholl JA, Garca-Etxarri A, Koh AL, Dionne JA. Observation of quantum tunneling between two plasmonic nanoparticles. Nano Lett 2013;13:564–9.
[33] Ciracì C, Chen X, Mock JJ, et al. Film-coupled nanoparticles by atomic layer deposition: comparison with organic spacing layers. Appl Phys Lett 2014;104:023109.
[34] Shen H, Chen L, Ferrari L, et al. Optical observation of plasmonic nonlocal effects in a 2D superlattice of ultrasmall gold nanoparticles. Nano Lett 2017;17:2234–9.
[35] Zhu W, Esteban R, Borisov AG, et al. Quantum mechanical effects in plasmonic structures with subnanometre gaps. Nat Comm 2016;7:11495.
[36] Raza S, Bozhevolnyi SI, Wubs M, Asger Mortensen N. Nonlocal optical response in metallic nanostructures. J Phys: Condens Mat 2015;27:183204.
[37] Raza S, Toscano G, Jauho AP, Wubs M, Asger Mortensen N. Unusual resonances in nanoplasmonic structures due to nonlocal response. Phys Rev B 2011;84:121412.
[38] Ullrich C. Time-dependent density-functional theory. Concepts and applications. Oxford, Oxford University Press, 2012.
[39] Zuloaga J, Prodan E, Nordlander P. Quantum description of the plasmon resonances of a nanoparticle dimer. Nano Lett 2009;9:887–91.
[40] Marinica DC, Kazansky AK, Nordlander P. Quantum plasmonics: nonlinear effects in the field enhancement of a plasmonic nanoparticle dimer. Nano Lett 2012;12:1333–9.
[41] Aguirregabiria G, Marinica D-C, Esteban R, Kazansky AK, Aizpurua J, Borisov AG. Role of electron tunneling in the nonlinear response of plasmonic nanogaps. Phys Rev 2018;97:115430.
[42] Barbry M, Koval P, Marchesin F, et al. Atomistic near-field nanoplasmonics: reaching atomic-scale resolution in nanooptics. Nano Lett 2015;15:3410–9.
[43] Baseggio O, De Vetta M, Fronzoni G, et al. Photoabsorption of icosahedral noble metal clusters: an efficient TDDFT approach to large-scale systems. J Phys Chem C 2016;120:12773–82.
[44] Xiang H, Zhang M, Zhang X, Lu G. Understanding quantum plasmonics from time-dependent orbital-free density functional theory. J Phys Chem C 2016;120:14330–6.
[45] D'Agostino S, Rinaldi R, Cuniberti G, Della Sala F. Density functional tight binding for quantum plasmonics. J Phys Chem C 2018;122:19756–66.
[46] Liu X, Seiffert L, Fennel T, Kühn O. A DFT-based tight-binding approach to the self-consistent description of molecule metal-nanoparticle interactions. J Phys B At Mol Opt Phys 2019;arXiv:1901.0374. in press. https://doi.org/10.1088/1361-6455/ab2b5d.
[47] Yan W. Hydrodynamic theory for quantum plasmonics: linear-response dynamics of the inhomogeneous electron gas. Phys Rev B 2015;91:115416.
[48] Toscano G, Straubel J, Kwiatkowski A, et al. Resonance shifts and spill-out effects in self-consistent hydrodynamic nanoplasmonics. Nat Comm 2015;6:7132.

[49] Ciracì C, Della Sala F. Quantum hydrodynamic theory for plasmonics: impact of the electron density tail. Phys Rev B 2016;93:205405.
[50] Ciracì C. Current-dependent potential for nonlocal absorption in quantum hydrodynamic theory. Phys Rev B 2017;95:245434.
[51] Khalid M, Ciracì C. Numerical analysis of nonlocal optical response of metallic nanoshells. Photonics 2019;6:39.
[52] Khalid M, Della Sala F, Ciracì C. Optical properties of plasmonic core-shell nanomatryoshkas: a quantum hydrodynamic analysis. Opt Express 2018;26:17322–8.
[53] Filter R, Bösel C, Toscano G, Lederer F, Rockstuhl C. Nonlocal effects: relevance for the spontaneous emission rates of quantum emitters coupled to plasmonic structures. Opt Lett 2014;39:6118–21.
[54] Christensen T, Yan W, Raza S, Jauho A-P, Asger Mortensen N, Wubs M. Nonlocal response of metallic nanospheres probed by light, electrons, and atoms. ACS Nano 2014;8:1745–58.
[55] Tserkezis C, Asger Mortensen N, Wubs M. How nonlocal damping reduces plasmon-enhanced fluorescence in ultranarrow gaps. Phys Rev B 2017;96:085413.
[56] Tserkezis C, Wubs M, Asger Mortensen N. Robustness of the Rabi splitting under nonlocal corrections in plexcitonics. ACS Photonics 2017;5:133–42.
[57] Manjavacas A, Garcia de Abajo FJ, Nordlander P. Quantum plexcitonics: strongly interacting plasmons and excitons. Nano Lett 2011;11:2318–23.
[58] Mortensen NA, Raza S, Wubs M, Søndergaard T, Bozhevolnyi SI. A generalized non-local optical response theory for plasmonic nanostructures. Nat Comm 2014;5:3809.
[59] de Ceglia D, Scalora M, Vincenti MA, et al. Viscoelastic optical nonlocality of low-loss epsilon-near-zero nanofilms. Sci Rep 2018;8:874.
[60] Ciracì C, Smith DR, Urzhumov YA. Far-field analysis of axially symmetric three-dimensional directional cloaks. Opt Express 2013;21:9397–406.
[61] Alpeggiani F, D'Agostino S, Claudio Andreani L. Surface plasmons and strong light-matter coupling in metallic nanoshells. Phys Rev B 2012;86:035421.
[62] D'Agostino S, Alpeggiani F, Claudio Andreani L. Strong coupling between a dipole emitter and localized plasmons: enhancement by sharp silver tips. Opt Express 2013;21:27602.
[63] Anger P, Bharadwaj P, Novotny L. Enhancement and quenching of single-molecule fluorescence. Phys Rev Lett 2006;96:113002.
[64] Gonçalves PAD, Christensen T, Rivera N, Jauho A-P, Asger Mortensen N, Soljačić M. Plasmon-emitter interactions at the nanoscale. 2019;arXiv:1904.09279.
[65] Gersten J, Nitzan A. Spectroscopic properties of molecules interacting with small dielectric particles. J Chem Phys 1981;75:1139–52.
[66] Ruppin R. Decay of an excited molecule near a small metal sphere. J Chem Phys 1982;76:1681–4.
[67] Tserkezis C, Stefanou N, Wubs M, Asger Mortensen N. Molecular fluorescence enhancement in plasmonic environments: exploring the role of nonlocal effects. Nanoscale 2016;8:17532–41.
[68] Moroz A. Non-radiative decay of a dipole emitter close to a metallic nanoparticle: importance of higher-order multipole contributions. Opt Commun 2010;283:2277–87.
[69] Delga A, Feist J, Bravo-Abad J, Garca-Vidal FJ. Quantum emitters near a metal nanoparticle: strong coupling and quenching. Phys Rev Lett 2014;112:253601–5.
[70] Jurga R, D'Agostino S, Della Sala F, Ciracì C. Plasmonic nonlocal response effects on dipole decay dynamics in the weak- and strong-coupling regimes. J Phys Chem C 2017;121:22361–8.
[71] Tserkezis C, Gonçalves PAD, Wolff C, Todisco F, Busch K, Mortensen NA. Mie excitons: understanding strong coupling in dielectric nanoparticles. Phys Rev B 2018;98:1–8.
[72] Chikkaraddy R, de Nijs B, Benz F, et al. Single-molecule strong coupling at room temperature in plasmonic nanocavities. Nature 2016;535:127–30.
[73] Stobbe S, Kristensen PT, Mortensen JE, Hvam JM, Mørk J, Lodahl P. Spontaneous emission from large quantum dots in nanostructures: exciton-photon interaction beyond the dipole approximation. Phys Rev B 2012;86:085304.
[74] Carnegie C, Griffiths J, de Nijs B, et al. Room-temperature optical picocavities below 1 nm^3 accessing single-atom geometries. J Phys Chem Lett 2018;9:7146–51.
[75] Ojambati OS, Chikkaraddy R, Deacon WD, et al. Quantum electrodynamics at room temperature coupling a single vibrating molecule with a plasmonic nanocavity. Nat Commun 2019;10:1049.
[76] Ciracì C, Rose A, Argyropoulos C, Smith DR. Numerical studies of the modification of photodynamic processes by film-coupled plasmonic nanoparticles. J Opt Soc Am B 2014;31:2601–7.
[77] Dung HT, Knoll L, Welsch DG. Spontaneous decay in the presence of dispersing and absorbing bodies: general theory and application to a spherical cavity. Phys Rev A 2000;62:053801.
[78] Ekardt W. Size-dependent photoabsorption and photoemission of small metal particles. Phys Rev B 1985;31:6360–70.
[79] Brack M. The physics of simple metal clusters: self-consistent jellium model and semiclassical approaches. Rev Mod Phys 1993;65:677–732.
[80] Olmon RL, Slovick B, Johnson TW, et al. Optical dielectric function of gold. Phys Rev B 2012;86:235147.